COBEM 2023 27TH INTERNATIONAL CONGRESS OF MECHANICAL ENGINEERING

ABCM Brazilian Society of Mechanical Sciences and Engineering
27th ABCM International Congress of Mechanical Engineering
December 04-08, 2023, Florianópolis-SC, Brazil

COB-2023-1947
STUDY OF THE PELTIER-SEEBECK EFFECT IN MIG WELDING PROCESS

Guilherme Amaral do Prado Campos
Adriane Lopes Mougo
Rodolfo do Lago Sobral
Cristiano de Souz a Carvalho
Joseph William Diniz Peixoto
Rodrigo Franco Côrtes

CEFET - RJ, Campus Nova Iguaçu, Rio de Janeiro, Brasil

guilherme.campos@cefet-rj.br
adriane.mougo@cefet-rj.br
rodolfo.sobral@cefet-rj.br
cristiano.carvalho@cefet-rj.br
joseph.peixoto@aluno.cefet-rj.br
rodrigo.cortes@aluno.cefet-rj.br

Abstract. *The Peltier-Seebeck thermoelectric effect refers to the generation of electricity from a temperature difference. The system that causes the heat flow to obtain this temperature difference is widely explored as an alternative to generate and supply energy in various electronic devices. The aim of this work is to carry out an initial study on the use of the welding process thermal cycle for energy generation by using Peltier module connected to the base metal. For this purpose, the KEMPI ProMIG 4200 welding machine, AWS ER70S-6 electrode wire with a diameter of 1.2 mm and A36 carbon steel plates with a 5 mm thickness were used. The applied welding machine parameters are listed as follows: voltage of 20.8 V, welding speed of 4.0 mm/s, electrode speed of 6.0 m/min and average current of 150 A. For the thermoelectric effect analysis, the equipment TEC1-12706 Peltier nodule, IMPLASTEC thermal paste, digital multimeter for voltage and current measurements, thermograph and heat exchanger were used. In view of the results obtained, it was possible to verify the possibility of applying Peltier module in energy generation from welding processes.*

Keywords: *peltier module, welding process, GMAW, renewable energy*

1. INTRODUCTION

The Peltier-Seebeck thermoelectric effect deals with obtaining electricity from a temperature difference. The system that induces the flow of heat to achieve this temperature difference is widely explored as an alternative to enable the generation and supply of energy in various electronic devices. This effect can be observed in practice through the use of Peltier cells or modules, which are employed as refrigerators or thermoelectric energy converters. Their structure consists of a small arrangement of blocks of Bismuth Telluride (Bi2Te3) doped with N-type and P-type semiconductors, soldered between two ceramic plates, electrically connected in series and thermally connected in parallel (Kakimoto, 2013; Luigi et al., 2021).

Some studies on the technological application of this electricity generated from Peltier modules have been presented for various daily household or industrial devices (Moura, 2010; Moraes, 2020). Additionally, these studies also present the sources of temperature difference generation (Slanina et al., 2018; Niedermaeyer, 2022; Torres, 2015).

In conventional welding processes, the heat generated by the electric arc is not fully utilized to melt the filler metal and form the fusion pool. Part of this heat is lost to the environment and, mainly, to the base metal through conduction. The heat flow in the base metal depends on some process parameters such as welding speed, voltage, and current, which are used to calculate the welding energy (Marques et al., 2009; Groover, 2012).

The welding energy, along with the initial temperature of the workpiece, are parameters that are easier for the operator to vary in order to control the cooling rate. When the cooling rate is too high, it tends to form embrittling microstructures in the welded material, such as the martensitic structure (Groover, 2012). Additionally, a low cooling rate enables the utilization of temperature to activate the Peltier-Seebeck effect when Peltier modules are connected along the base metal.

Based on this consideration, this study aims to conduct an initial investigation into harnessing the thermal cycle of the welding process for energy generation using Peltier cells connected to the base metal. For this purpose, an experimental

plan will be proposed, adapted to the limitations of temperature acquisition during the welding process and the capacity of the Peltier module. Additionally, the geometric aspects of height and width measured along the weld bead will be presented.

2. EXPERIMENTAL PLANNING

For the welding process conducted in this study, a KEMPI ProMIG 4200 welding machine, AWS ER70S-6 electrode wire with a diameter of 1.2 mm, and ASTM A36 steel plates with dimensions of 800 mm X 300 mm X 5 mm were used.

For the analysis of the thermoelectric effect, the Peltier module TEC1-12706 (TEG-Thermoeletric Generator) was employed, along with thermal paste from IMPLASTEC to secure the module to the base metal. A digital multimeter was used for voltage measurements, a thermographic camera for temperature readings, and a heat exchanger to enhance the temperature difference in the system for one of the modules.

This TEC1-12706 Peltier module is made of ceramic sealed with industrial silicone, with an approximate power consumption of 91 W, resistance of $1.3 - 1.5$Ohm, and operating temperature range from 30°C to 130°C. Figure 1 illustrates the main equipment of the data acquisition system.

Figure 1. MIG power source, KEMPI ProMIG 4200, Peltier module TEC1-12706 and thermal camera

Figure 2 shows the assembly of the experimental setup. On the right side of the weld bead, it is possible to observe the base metal with 5 Peltier modules positioned longitudinally and transversely, with ammeters connected to measure the voltage during the cooling of the workpiece. The distance between Peltier modules 1, 2, and 3 from the weld bead was 10 cm, while the distance between these modules was 5 cm. This same distance was also used to position modules 4 and 5 relative to module 2.

Considering that the distribution of heat flow through conduction remains symmetrical on both sides of the weld bead along the base metal, Peltier module 6 was positioned on the left side of the weld bead, in the same location as module 2, with the aim of comparing energy generation with the aid of a heat sink.

The recorded open arc time was 68 s, and the length of the weld bead was 270 mm, resulting in a welding speed of approximately 4.0 mm/s. The welding parameters used were a wire feed speed of 6 m/min, a voltage of 20.8 V, and a current of approximately 150 A.

3. NUMERICAL FORMULATION

In this section the mathematical description for the heat transfer process in rigid and opaque body in the rest will be present employing the classical form of the physical laws. The nonlinear problem presented will be solved starting from the limit of a sequence whose elements are linear problem solutions (Gama, 1997).

3.1 Mathematical Model

Equation (1) denotes the partial differential equation of heat conduction in generic coordinate system (Ozisik, 1993).

$$\nabla \left[k \nabla T\left(r,t\right)\right] + g\left(r,t\right) = \rho C_p \frac{\partial T\left(r,t\right)}{\partial t} \quad in \quad \Omega \tag{1}$$

whith k material thermal conductivity, T the absolute temperature, g internal energy generation, ρ density and C_p thermal capacity.

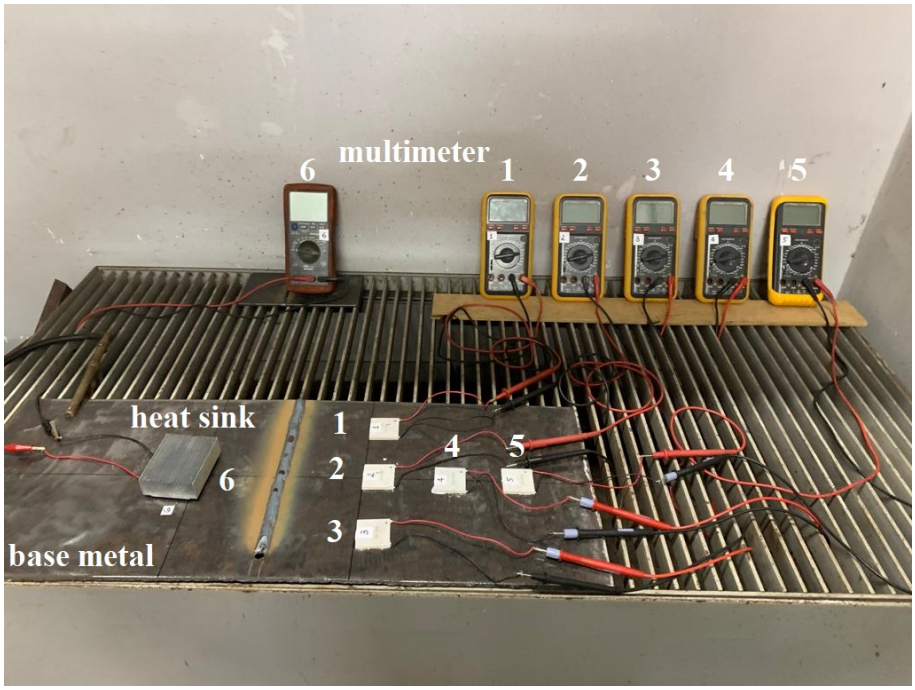

Figure 2. Experimental apparatus

The coupling between the conduction heat transfer, convection and thermal radiation heat transfer is done on the body boundary. For a black convex body with emissivity $\epsilon = 1$ surrounded by an atmosphere-free space, since there is no jump in the normal energy flux across the boundaries $\partial\Omega$, in real conditions, we must have nonlinearity on the boundary condition, such as Eq. (2):

$$-k\nabla T.\mathbf{n} = \sigma|T|^3T + h(T - T_\infty) \;\; on \;\; \partial\Omega \tag{2}$$

in wich $\mathbf{n}$ is the unit outward normal vector, σ is the Stefan-Boltzmann constant, T_∞ is a temperature of reference (in general, the enviroment temperature) and h is the convection heat transfer coefficient.

3.2 Numerical Methodology

The nonlinear problem presented in Eq. (2) will be solved starting from the limit of a sequence whose elements are linear problem solutions. Gama (1997 and 2023) explains and prove the constructing the sequences $[\Psi_0, \Psi_1, \Psi_2, ..., \Psi_i]$ with the limit of this sequence satisfing the Eq. 1), as showed in Eq. (3 and 4):

$$div(\nabla\Psi_i) + \frac{g(\mathbf{r})}{k} = 0 \quad in \quad \Omega \tag{3}$$

$$-k\frac{\partial\Psi_i}{\partial r} = \gamma\Psi_i - \left(\gamma\Psi_{i-1} - \sigma|\Psi_{i-1}|^3\Psi_{i-1} - h(\Psi_{i-1} - T_\infty)\right) \quad on \quad \partial\Omega \tag{4}$$

with $T = \lim_{i\to\infty}\Psi_i$, the term $|\Psi_{i-1}|^3\Psi_{i-1}$ is the coercitivity term that ensures the existence of at least one solution.

The problem proposed in its originality has boundary condition type Robin, but the proposed methodology simplifies way on the convergence of the solution, imposing a boundary condition of Neumann type without physical meaning, but rather as a effective mathematical tool. Equation (5) presented the auxiliar term β:

$$\beta_i = \gamma\Psi_{i-1} - \left(\sigma|\Psi|^3\Psi_{i-1} - c + h(\Psi_{i-1} - T_\infty)\right) \tag{5}$$

Rewriting the Eq. (3) and Eq. (4) with respect β, have the Eq. (6 and 7),

$$div(kgrad\Psi_{i+1}) + \dot{q} = 0 \quad in \quad \Omega \tag{6}$$

$$-kgrad\Psi_{i+1}.\mathbf{n} = \gamma\Psi_{i+1} - \beta_i \quad on \quad \partial\Omega \tag{7}$$

for $\Psi_0 \equiv 0$, the sequence $[\Psi_0, \Psi_1, \Psi_2, ..., \Psi_i]$ converges in $\partial\Omega$, Gama (2022) makes the analytical demonstration of this series.

4. RESULTS AND DISCUSSION

The analysis and processing of all the data, methods and processes exposed in this work have resulted in some extremely relevant conclusions. Since this work argues that certain phenomena can not be neglected, all simulation procedures occurred contemplating the most varied situations so that it is possible to make comparisons of the results and determine the relevance of the study. The simulation environment was maintained in all situations, except for the parameters that characterize the preponderant differences that will be compared. Table 1 presents the parameters applied and obtained in this study using the commercial software Matlab, allowing the analysis of the algorithm results via mathematical data and graphical information so that quantitative analysis is possible through thermal mapping of thermoelectric energy generation. It is worth mentioning that the parameters stipulated can be handled in a convenient manner in order to

Table 1. Applied and obtained parameters

Symbol	Concept	Value
T_∞	Reference Temperature	$300K$
T_{ad}	Adjusted weld bead temperature	$449.32K$
$i\mathbf{x}j$	Mesh Size	$60\mathbf{x}60$
Tol	Specified Accuracy	$1e-6$
γ	Convergence Parameter	$1e4$
n	Linear Iteration Number	15885
n'	Nonlinear Iteration Number	12463

investigate results in other circumstances. In order to allow better visualization and understanding of the obtained results, some descriptive tables were generated. In order to verify the numerical convergence methodology, the algorithm was validated for three different values of the convergence parameter.

4.1 Experimental

Table 2 presents the temperature values measured on the weld bead and the voltage values measured for the modules every 10 seconds. It can be observed that from 130 seconds (2 minutes and 10 seconds) onwards, the temperature and voltage values of modules P1, P2, and P3 start to decrease, while the voltage in module P6, with a heat sink, continues to increase until approximately 240 seconds (4 minutes). Modules P4 and P5 did not show significant variation in voltage during the cooling of the weld bead. Therefore, for the next experiments, energy generation with the aid of a heat sink will be verified for the modules located farther from the weld bead.

Voltage measurements were performed up to 10 minutes. Even at this maximum time, with the voltage dropping, module P6 showed a value of 0.355 V, which is higher than the highest voltage generated by module P2 (0.194 V at a temperature of 213.6°C). Figure 3 shows the graph of voltage variation over time for modules P1, P2, P3, and P6. The first three modules exhibit a similar voltage behavior: the voltage increases until approximately 130 seconds and then stabilizes. Module P6, with a heat sink, shows an increase in voltage until 200 seconds and then starts to decline.

Another important observation made was the higher voltage measured by module P2 compared to modules P1 and P3, as shown in the example in Fig. 4. This can be explained by the phenomenon of natural conduction and convection, which occurs along the plate during the welding process and exposure to the environment. When observing the top and bottom of the modules, they are considered to be under the same conduction and convection condition. However, when analyzing the sides of the modules, they are affected differently due to natural convection. In the case of module P2, the plate can be considered infinite, with only heat conduction occurring, and there is no significant influence from the lateral edges, resulting in higher voltage values. On the other hand, modules P1 and P3 are closer to the lateral edges of the plates, modifying the heat dissipation due to natural convection and conduction. This proximity to the lateral edge alters the temperature difference, resulting in lower voltages.

The maximum temperature measured in the experiment occurred at the moment of opening the weld bead and was recorded at $476°C - 749.5K$. In the following section, the numerical modeling of the empirical process will be described by calculating a simple average of the empirical temperature values (T_{ad}) in order to simplify and fix the initial temperature in the weld bead.

4.2 Thermal Mapping

This section will address the numerical results regarding the thermal mapping of cast sheets using an external thermal source in the weld bead. The analytical partial differential equations were modeled numerically in previous section and their solution will be presented in the context of linear and non-linear boundary conditions so that results can be compared.

Thermal conductivity was adopted as a constant and the effect of mutual thermal radiation was neglected. The mesh

Table 2. Variation of voltage with time and temperature of the weld bead

Time (s)	T (°C)	P1 (V)	P2 (V)	P3 (V)	P4 (V)	P5 (V)	P6 (V)
0	476	0,069	0,019	-0,008	-0,003	-0,002	0,0156
10	149,7	0,097	0,059	0,008	-0,002	-0,002	0,0639
20	135,7	0,113	0,086	0,026	-0,002	-0,002	0,1294
30	128,3	0,129	0,114	0,051	-0,001	-0,001	0,2111
40	123,5	0,143	0,141	0,081	0	-0,001	0,2927
50	109,9	0,152	0,164	0,113	0	0	0,3816
60	306,2	0,155	0,177	0,129	0,001	-0,001	0,466
70	234,8	0,158	0,187	0,143	0,003	0,001	0,547
80	213,6	0,158	0,194	0,161	0,005	0,001	0,621
90	223,9	0,157	0,192	0,168	0,007	-0,001	0,689
100	204	0,154	0,191	0,171	0,01	-0,001	0,748
110	179,2	0,151	0,188	0,17	0,012	-0,001	0,798
120	168	0,145	0,187	0,17	0,015	0	0,843
130	170,7	0,142	0,181	0,167	0,018	0	0,883
140	178,6	0,135	0,171	0,162	0,02	0	0,913
150	171,3	0,129	0,162	0,158	0,021	0	0,937
160	155,8	0,123	0,155	0,149	0,022	0	0,955
170	160,9	0,122	0,152	0,148	0,025	0	0,967
180	143	0,119	0,147	0,143	0,027	0	0,975
190	148,6	0,114	0,141	0,134	0,028	0	0,98
200	138,6	0,113	0,137	0,132	0,029	0,001	0,98
210	124,4	0,11	0,129	0,125	0,029	0,001	0,977
220	125,1	0,108	0,124	0,123	0,03	0,002	0,972
230	116,3	0,104	0,119	0,119	0,033	0,003	0,964
240	109,6	0,101	0,119	0,115	0,034	0,003	0,955

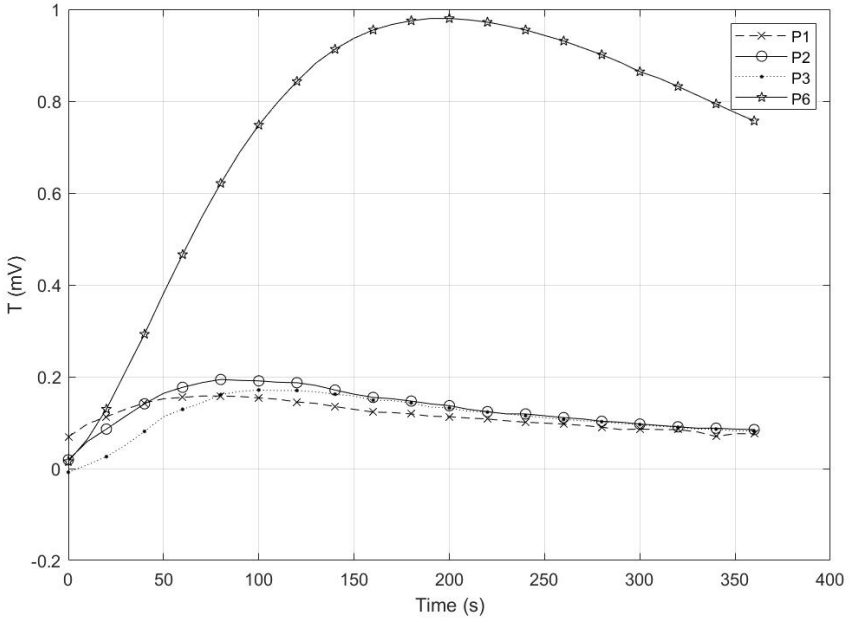

Figure 3. Voltage variation over time

is made up of 60x60, reference temperature of $T_\infty = 300K$, Stefan Boltzman constant $\sigma = 1.10^{-4} W/m^{-2}K^{-4}$, the thermal conductivity (k) and the heat transfer coefficient (h) of the base metal are $51.9W/mK$ and $10W/mm^2K$, respectively. The simulation is represented by uniform, structured and cartesian grid, a mesh with evenly spaced points. Intuitively, the greater the number of discrete points, that is, the finer mesh is most faithful model in the numerical result.

Figure 4. Multimeters

It is to be noticed that the convergence was reached for $\gamma = 1e4$. In other words, for values greater than $\gamma = 1e4$ no significant changes were observed. Figure 5 (i) expresses the thermal mapping for convection boundary conditions, (ii) the thermal mapping for convection-radiation boundary conditions and (iii) overlays these results.

Simplifications regarding the numerical solution methodology with linear boundary conditions denote faster results prediction times, however Tab. 3 presents the relevance of the radiation phenomenon as a boundary condition, note that percentage errors around almost 10% are obtained by neglecting this effect. Such errors can be aggravated in conditions of higher weld bead temperatures or in a controlled/rare atmosphere, situations where the phenomenon of radiation prevails in heat dissipation.

Table 3. Linear vs Nonlinear boundary condition

Node Temperature	Linear	Nonlinear	%Error
1	$450K$	$450K$	0
5	$446.6723K$	$440.6091K$	1.35
10	$442.8774K$	$430.1529K$	2.87
15	$439.4780K$	$421.0060K$	4.20
20	$436.4647K$	$413.0649K$	5.36
25	$433.8293K$	$406.2437K$	6.35
30	$431.5642K$	$400.4713K$	7.20
35	$429.6634K$	$395.6897K$	7.90
40	$428.1216K$	$391.8522K$	8.47
45	$426.9344K$	$388.9222K$	8.90
50	$426.0986K$	$386.8722K$	9.20
55	$425.6120K$	$385.6833K$	9.38
60	$425.4730K$	$385.3445K$	9.43

According to TEC12701 datasheet the mV voltage output occurs according to the variation in temperature between the hot-cold faces of the TEG, Fig. 6 (i) clarifies this relationship. In order to extrapolate voltage values to different other temperature ranges, the least squares method by polynomial curve fitting was calculated and the Eq. (8) was defined as numerical methodology.

$$f(x) = -0.0698x^2 + 43.3541x + 71,6058 \tag{8}$$

with x the temperature difference in$^{\circ}C$ and $f(x)$ the voltage output in mV.

The data shows that the voltage increases with temperature difference. The voltage may be higher if the Seebeck coefficient is higher, considering the numerical values obtained for the plate hot face and using thermograph data, Fig. 6 (ii) relates the voltage calculated for 0, 30, 60, 90, 120, 150, 180, 210 and 240 seconds on $P6$ ratifying the empirical data obtained in Tab. 2.

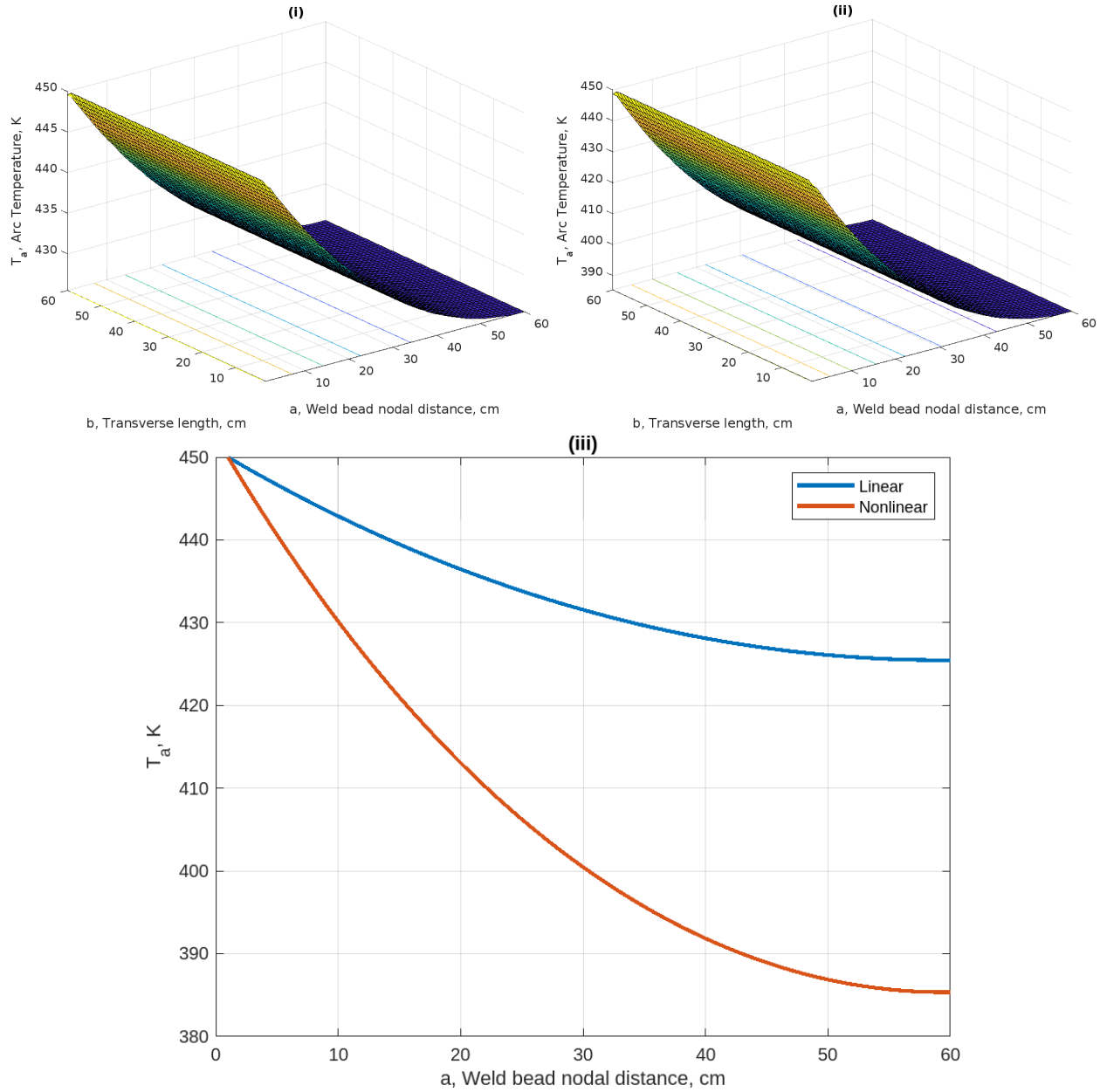

Figure 5. Thermal mapping (i) Linear boundary condition; (ii) Nonlinear boundary condition and (iii) Overlap linear vs nonlinear temperature

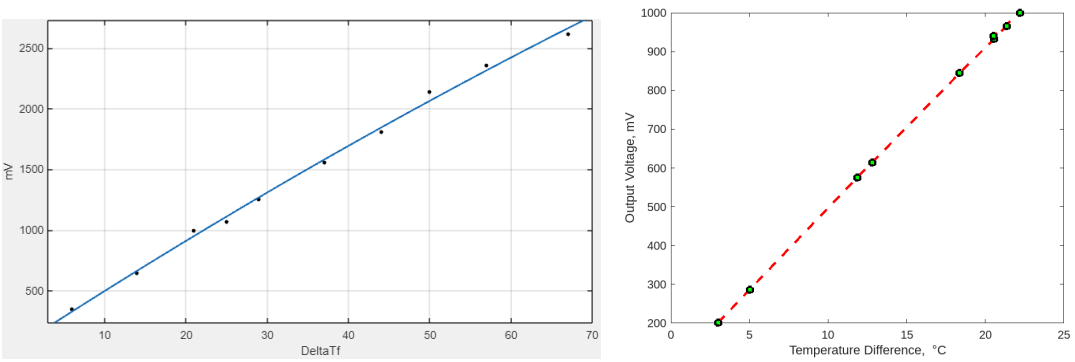

Figure 6. (i) Datasheet TEC12706 curve fitting with least square method; (ii) Calculated thermoelectric generation for $P6$

5. CONCLUSIONS

This study aims to investigate the energy generation through the Peltier-Seebeck effect in the MIG welding process. In these initial tests, different positions of the Peltier modules relative to the weld bead and the use of heat sinks were examined to assess the variation of voltage generated. From this preliminary stage, the following conclusions were drawn:

- Modules positioned at 15 cm and 20 cm (P4 and P5) from the weld bead did not show a significant variation in measured voltage compared to the other modules located 10 cm from the weld bead. For this situation, it is considered to use heat sinks in the next experiments.
- Modules P1, P2, and P3 exhibited an increase in voltage until approximately 100 seconds, which coincides with the beginning of the temperature drop.
- Module P6, with a heat sink, showed this voltage increase until approximately 200 seconds. However, over the total 10 minutes of measurement, the voltage generated by this module exceeded the highest voltage measured in module P2, without a heat sink.
- Module P2 displayed a higher voltage compared to modules P1 and P3 because P2 is not influenced by natural convection at the lateral edges, while P1 and P3 are directly affected, reducing the temperature difference and consequently generating less voltage.

The work presents the relevance of using entropy in the MIG welding process in thermoelectric generation, taking scientific computing as a counterpoint to predict thermal mapping and its potential for entropy reduction. Possible empirical-numerical discrepancies are due to inaccuracies in numerical linearization, non-ideal measurement conditions and human errors in carrying out technical procedures.

6. REFERENCES

Bernardo, R. T. Desenvolvimento de uma plataforma para aplicação de técnicas de controle de temperatura por efeito peltier. 2015. Trabalho de conclusão de curso (Bacharelado em Engenharia de Controle e Automação) - Universidade Federal de Ouro Preto, Ouro Preto, 2015.

Gama, R.M.S., 1997. The nonlinear conduction/radiation heat transfer phenomenon represented as the limit of a sequence of linear problems. International communications in heat and mass transfer, Vol. 24, No. 1, pp. 119–128.

Gama, Rogério Martins Saldanha da. The Heat Transfer Problem in a Non-Convex Body—A New Procedure for Constructing Solutions. Axioms, v. 12, n. 4, p. 338, 2023.

Gama, Rogério Martins Saldanha da. A Very Simple Procedure for Constructing the Solution of Nonlinear Elliptic PDEs (with Nonlinear Boundary Conditions) Arising from Heat Transfer Problems in Solids. Axioms, v. 11, n. 7, p. 311, 2022.

HAKIM, Ameer; LIM, Joon Hoong. The effect of temperature mismatch on interconnected thermoelectric module for power generation. In: AIP Conference Proceedings. AIP Publishing, 2020.

Kakimoto, L. C. Efeito Peltier-Seebeck: gerando eletricidade por diferença de temperatura. Campinas, 2013. 55 f. TCC – Instituto de Física Gleb Wataghin, Unicamp, Campinas, 2013.

Luigi, O. F., Luis M. N., Byron P. C., Jessica N. C., Efficiency in thermoelectric generators based on Peltier cells, Energy Reports, Volume 7, Supplement 3, 2021, Pages 355-361, ISSN 2352-4847.

Marques, P. V., Modenesi, P. J., Bracarense, A. Q. Soldagem Fundamentos e Tecnologia, 3ª edição, Editora UFMG, 2009. Groover, M. P. Introdução aos processos de fabricação. GEN LTC, 2012.

Moraes, R. S., Guilherme, A. P. Aprendizagem de Conceitos Físicos a Partir daConstrução de uma Mini Geladeira de PastilhaPeltier. Revista do Professor de Física, v. 4, n. 3, p. 84-97, Brasília, 2020. Instituto de Física - Universidade de Brasília.

Moura, J. A. S. Filmes Nanométricos de FeN e AIN Crescidos por Sputtering e Aplicações do Efeito Peltier. 2010. Tese (Doutorado em Física Teórica e Experimental) - Universidade Federal do Rio Grande do Norte.

Niedermayer, A. C. Desenvolvimento de um Sistema de Aquecimento Controlado: Uma aplicação da pastilha de Peltier. Trabalho de Conclusão de Curso. Universidade Tecnológica Federal do Paraná, 2022.

Ozisik, M.N., 1993. Heat conduction. John Wiley & Sons.

Zdenek, S., Martin U., Vaclav S., Cooling Device with Peltier Element for Medical Applications, IFAC-PapersOnLine, Volume 51, Issue 6, 2018, Pages 54-59, ISSN 2405-8963.

7. RESPONSIBILITY NOTICE

The following text, properly adapted to the number of authors, must be included in the last section of the paper:
The author(s) is (are) solely responsible for the printed material included in this paper.